engineering proceedings

MDPI

Proceeding Paper

Adaptive Owl Search Optimisation for Real-Time Fault-Resilient Control of DFIG-Integrated Wind Energy Systems †

Ramesh Kumar Behara and Akshay Kumar Saha *

Electrical, Electronic, and Computer Engineering, University of KwaZulu-Natal, Durban 4041, South Africa; bramesh250770@gmail.com or 222131240@stu.ukzn.ac.za

* Correspondence: saha@ukzn.ac.za; Tel.: +0027-31-260-2725-2305

† Presented at the 34th Southern African Universities Power Engineering Conference (SAUPEC 2026), Durban, South Africa, 30 June–1 July 2026.

Abstract

The rapid global deployment of wind energy requires robust and efficient control strategies for doubly fed induction generator (DFIG)-based systems. Conventional proportional–integral (PI) controllers tuned by classical or metaheuristic methods often exhibit poor adaptability to turbulence, parameter drift, and grid disturbances. This paper introduces an adaptive owl search optimisation (A-OSO) algorithm for the real-time tuning of PI controllers in DFIG back-to-back converters. Unlike traditional OSO, the adaptive variant dynamically adjusts its exploration–exploitation balance based on the severity of system disturbances, enabling faster convergence and improved resilience. The study benchmarks the proposed method against particle swarm optimisation (PSO), genetic algorithm (GA), simulated annealing (SA), and owl search optimisation (OSO) simulation studies in MATLAB/Simulink, coupled with hardware-in-the-loop (HIL) tests on an FPGA platform, demonstrating that A-OSO achieves superior efficiency (97.1%), lower power losses (35 kW), faster low voltage ride-through (LVRT) recovery (less than 150 ms), and reduced total harmonic distortion (THD) (2.4%). These findings establish A-OSO as a practical, grid-compliant optimisation strategy for next-generation smart wind farms.

Keywords: doubly fed induction generator; owl search optimisation; particle swarm optimisation; simulated annealing hardware-in-the-loop; cyber-attack emulation; MATLAB

1. Introduction

Wind power plays a central role in the global energy transition [1]. DFIG-based wind turbines dominate modern installations because they use partially rated converters (25–30% of rated power) and enable the independent control of active and reactive power. However, their nonlinear and time-varying dynamics, driven by fluctuating wind conditions and grid disturbances [2], demand robust controller tuning. Although conventional PI controllers are simple to implement, they become vulnerable to instability when tuned manually or using gradient-based methods [3]. Metaheuristic methods such as PSO, GA, and SA enhance adaptability, but they still face challenges, including premature convergence, high computational burden, and limited resilience under fault conditions [4,5].

Recent works introduced intelligent methods, including reinforcement learning (RL) [6] and adaptive neuro-fuzzy inference systems (ANFIS-PI) [7], which offer enhanced adaptability but at the cost of computational complexity and black-box behaviour. In reference [8], the study introduces a passive sliding-mode layer to the RSC enhancing

Check for updates

Academic Editor: Remy Tiako

Published: 5 June 2026

Copyright: © 2026 by the authors. Licensee MDPI, Basel, Switzerland. This article is an open access article distributed under the terms and conditions of the Creative Commons Attribution (CC BY) license.

LVRT. Meanwhile, recent work reports HIL wind-controller implementations that validate timing and stability under realistic constraints, aligning with grid-code practice as per IEEE 1547-2018 [9] and its regional adaptations. OSO, inspired by owls' hunting strategies, provides a promising balance of exploration and exploitation. Early OSO studies reported success in benchmark problems and control tasks [10]. Yet, its direct application to DFIG converter optimisation remains limited. Furthermore, OSO has not been extended to real-time adaptive scenarios or validated beyond simulations. Reference [11] models false data injection (FDI), denial of service (DoS)/jamming, and hijack attacks on DFIGs, with HIL co-simulation validating the defences (learning-based and modified backstepping).

1.1. Research Gap

Despite notable advances in controller optimisation for DFIG-based wind energy systems, several gaps remain. Existing metaheuristic methods offer limited real-time adaptability to abrupt grid disturbances and wind variability, constraining their practical effectiveness. Moreover, most studies prioritise efficiency while overlooking multi-objective trade-offs among THD, LVRT compliance, and computational complexity, limiting their relevance to smart grid operation. Finally, the study validates the approach primarily through simulations and does not sufficiently consider real-time implementation or scalability for utility-scale wind farms.

1.2. Contribution

This paper addresses these gaps by proposing an A-OSO framework for PI tuning in DFIG converters. The approach introduces a disturbance-aware exploration–exploitation mechanism that dynamically adjusts the search strategy to the operating conditions. A multi-objective fitness function balances efficiency, THD, LVRT compliance, and computational cost, enabling holistic optimisation. The framework is validated through MATLAB R2025b simulations and HIL experiments and is benchmarked against PSO, GA, SA, and OSO-PI, demonstrating superior adaptability, robustness, and computational efficiency.

The paper proceeds as follows: Section 2 presents the proposed framework; Section 3 describes the methodology; Section 4 reports the simulation results; Section 5 compares performance and discusses the results; and Section 6 concludes the paper and outlines future work.

2. Proposed Framework

2.1. System Model

Figure 1 depicts the overall DFIG wind energy conversion system, comprising a mechanical drive train and an electrical conversion stage. The gearbox mechanically couples the wind turbine to the DFIG rotor; the stator connects directly to the grid; and a back-to-back converter, comprising an RSC, a DC-link capacitor, and a GSC, interfaces the rotor with the grid. The RSC regulates active and reactive power through rotor-current control, while the GSC maintains the DC-link voltage and controls grid-current injection. PI gains for both converters are adaptively tuned using owl search optimisation to improve dynamic performance and fault resilience.

As illustrated in Figure 1, the diagram maps the interaction pathways within the co-simulation environment. The arrows originating from the Genetic Algorithm (GA) Optimization Framework box denote the spatial allocation, sizing directives, and controller tuning gains computed by the master shell in MATLAB and injected into the PSCAD EMT environment. Within the network layout, the bold horizontal and vertical lines connecting the nodes trace the physical power flow paths of the modified IEEE 33-bus active distribution system. Furthermore, the arrows intersecting the primary buses with

the peripheral generation and load blocks represent bidirectional active and reactive power transformations (P-Q intersections). Finally, the returning dashed and solid pathways establish the closed-loop feedback path, routing the real-time EMT measurements from the PSCAD environment back to the GA optimization engine.

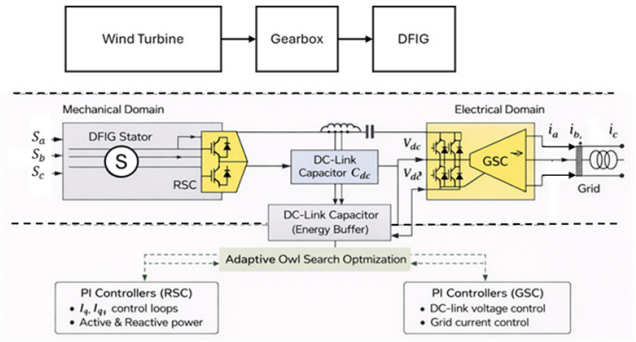


Figure 1. System architecture of the integrated DFIG wind turbine with the grid.

2.2. Adaptive OSO (A-OSO)

An A-OSO balances exploration and exploitation, but uses static hyperparameters which limit responsiveness to turbulence and voltage sags in DFIG control [12]. The study introduced an A-OSO with a real-time disturbance index (DI) [13] (from rotor-speed variance, DC-link ripple, and grid-voltage deviation) that scales step size/inertia: low DI, exploitation (fine-tuning PI gains); high DI, (exploration + diversity) to prevent premature convergence and speed recovery, consistent with recent adaptive intelligent-control trends [14,15]. A-OSO minimises a multi-objective cost *J*, includes DI-tied evaluation budgets for real-time execution, and explicitly targets ride-through behaviour aligned with DFIG disturbance handling in the literature [16]. Embedded/HIL precedents for advanced DFIG controllers support the feasibility of the proposed loop [1].

2.3. Multi-Objective Cost Function

This study defines the optimisation task as a multi-objective control problem in which the A-OSO algorithm simultaneously enhances system performance, power quality, and fault resilience [17]. To achieve this, study [16] formulated a composite cost function *J* by combining the integral of time-weighted absolute error (ITAE), overshoot (OS), settling time T_s, power loss, THD, and LVRT score capability as:

$$J = w_1 \cdot ITAE + w_2 \cdot OS + w_3 \cdot T_s + w_4 \cdot P_{Loss} + w_5 \cdot THD - w_6 \cdot LVRT_{SCORE} \quad (1)$$

The authors chose the A-OSO parameters to balance control performance and real-time feasibility. The objective–function weights in Equation (1) emphasise fast active-power recovery and DC-link voltage regulation while limiting current and control effort. A population size of $N = 20$ ensures sufficient search diversity while maintaining low computational overhead, and we set the iteration count and convergence tolerance to guarantee timely convergence within the controller update interval.

2.4. Algorithm Steps

The algorithm initialises an owl population of candidate PI gains within admissible bounds and sets N, $I_{\max}$, tolerance ε, and a real-time evaluation budget. The study evaluates each candidate using the DFIG model to compute the composite cost J, updating personal and global bests. A normalised disturbance index (DI), derived from rotor-speed variance, DC-link voltage ripple, and grid-voltage deviation, governs adaptation. High DI increases exploration via a scaling factor, γ, while low DI promotes exploitation around the best

solution within the computational budget. Owl positions are updated using OSO dynamics, projected within limits, and re-evaluated with elitism. The algorithm terminates the process when improvement falls below ε or when it reaches the iteration limit or budget, after which the controller deploys the best gains to the RSC and GSC.

The algorithm section focuses on control-oriented DFIG dynamics for optimisation purposes. The model represents the back-to-back converters, DC-link, filter, and transformer using average-value models and neglects switching dynamics to ensure real-time feasibility. Low-frequency power and voltage dynamics govern the disturbance index and therefore prevent high-frequency converter phenomena from affecting it. In this work, DC-link ripples refer to the low-frequency oscillations of the DC-link voltage.

3. Methodology

3.1. Simulation Platform

The authors conducted offline experiments in MATLAB/Simulink R2022b (SimPowerSystems) using common random seeds, identical initial conditions, and uniform evaluation horizons of 10–20 s across scenarios. The study logged data at 10 kHz and averaged KPIs over the last (3–5) seconds of each operating segment. The study consistently applied LVRT sags and cyber impairments across all methods to enable apples-to-apples comparison and support real-time feasibility on FPGA/HIL.

The authors modelled a 2 MW DFIG with a sixth-order machine (stator/rotor leakage inductance, magnetising inductance, pole pairs, and copper losses) and parameterised it using typical manufacturer data. This study included back-to-back VSCs with PWM at 5–10 kHz and sized the DC-link to keep the voltage ripple <1% at nominal swing. The study tuned the RSC/GSC inner/outer PI gains online via A-OSO; a DI, derived from windowed rotor-speed variance, sliding-RMS DC-link ripple, and PCC-voltage deviation, drives the exploration–exploitation scaling γ and the evaluation budget. The authors simulated the modelling in a discrete-time power stage (Δt = 20–50 µs) and controller task (100–200 µs), and reported results using the discrete solver to mirror HIL timing.

3.2. Flow Chart of the Modified A-OSO

Figure 2 shows that the modified A-OSO performs the online tuning of RSC/GSC PI gains in a DFIG by augmenting the standard OSO with a DI that adaptively balances exploration/exploitation, and schedules computation. Starting with inputs, measured signals $\{\omega_r, v_{dc}, v_{pcc}, i_{dq}\}$, PI bounds $[K_{\min}, K_{\max}]$, cost weights w, population size N, iteration cap $I_{\max}$, tolerance ε, period, and a real-time budget, the algorithm initialises (F1) N candidate gain vectors within bounds, evaluates them once, and sets personal/global bests (p_i, and g). Each control cycle senses and buffers windows of the required measurements (F2). It then computes the DI (F3) from features such as rotor-speed variance, DC-link RMS ripple, and PCC-voltage deviation, normalises and low-pass filters them to obtain DI $\in [0, 1]$, and flags dropouts/jams via hold-last-sample logic. The controller maps the DI (F4) to adaptation knobs, the step/inertia scale γ, the exploration weight β, and the evaluation budget B, and widens the bounds around g to permit diversity injections when DI > τ. OSO parameters are updated accordingly (F5). Each owl is then evaluated (F6) over a short horizon with the multi-objective cost as explained in "(1)", while logging secondary KPIs and debiting the budget. Personal and global bests are refreshed (F7), and positions are moved (F8) via OSO kinematics scaled by γ:

$$x_i^{k=1} = x_i^k + \gamma\left[\beta r_i\left(g - x_i^k\right) + (1-\beta)\varepsilon_i\right] \quad (2)$$

with repair/clipping and PI anti-windup limits enforced. If $DI > \tau$ or stagnation persists for H iterations (F9), the method injects diversity, local jitter for strong candidates, and reinitialises the worst ρ%, shrinking again when DI falls. The algorithm terminates (F10) when improvement remains below ε for H steps, when it exhausts I_{max} or B, or when it reaches a hard deadline; otherwise, the loop continues. Upon termination, the controller deploys the current best gains to the RSC/GSC (F11) and logs the KPIs and DI. The cycle then proceeds (F12) with sliding windows, the periodic widening of bounds, the reseeding of the diversity pool, and the archiving of g.

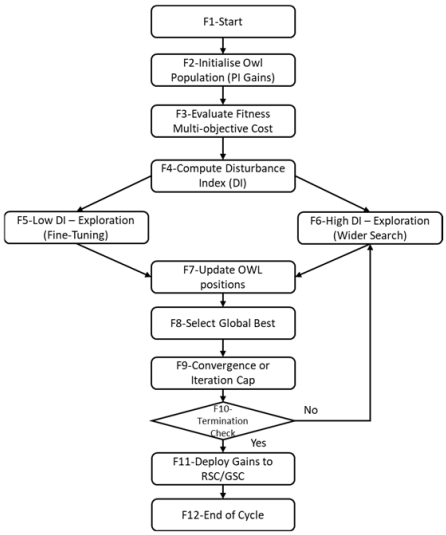


Figure 2. Flow Chart of modified OSO.

3.3. HIL (Hardware-in-Loop) Platforms

Real-time validation used a Xilinx Field-Programmable Gate Array (FPGA) with a 20 µs simulation step, interfaced to an RTDS-class simulator via isolated I/O. The DFIG plant ran in fabric at 50 kHz, the control stack executed in a soft-core/FPGA co-design, with DI/cost paths optionally pipelined in digital signal processing (DSP) slices. The authors used fixed-point (Q-format) arithmetic and cross-checked it against floating-point Simulink. The study set the scaling to avoid overflow up to 1.2 pu. Simulator-emulated analogue inputs fed the controller; digital outputs drove PWM duty cycles and GSC setpoints. End-to-end control latency was <2 ticks with <1 tick jitter. A watchdog-backed real-time scheduler enforces timing, while PI bounds, overcurrent/overvoltage trips, and scripted voltage sag injection provided protection.

3.4. Cyber-Attack Emulation (Jamming/Delay)

The authors emulate communication-layer faults on RSC/GSC feedback signals (v_{dc}, i_{dq}, ω_r, v_{pcc}). They inject a delay as deterministic first-in-first-out holds of $d \in \{0.5, 1, 2\}$ control ticks (100–200 µs) with optional ± 0.1-tick jitter. Packet loss follows (a) Bernoulli drops ($p \in \{1, 3, 5\}$%) with zero-order hold and (b) burst jamming using a two-state Gilbert–Elliott model (100–300 ms mean bursts within random 4–16 s windows). All controllers reject outliers and hold the last sample, while A-OSO computes its DI from corrupted measurements. Each scenario runs with $n = 10$ seeds over a 10–20 s horizon, a 20–50 µs step size, and 10 kHz logging. KPIs include dynamic response (ΔTs, overshoot, ITAE), power quality (THD@PCC, PF), efficiency and power losses, fault resilience (spurious trips, recovery), and computational footprint (iterations/round, DI trajectory, latency/WCET).

4. Simulation Results

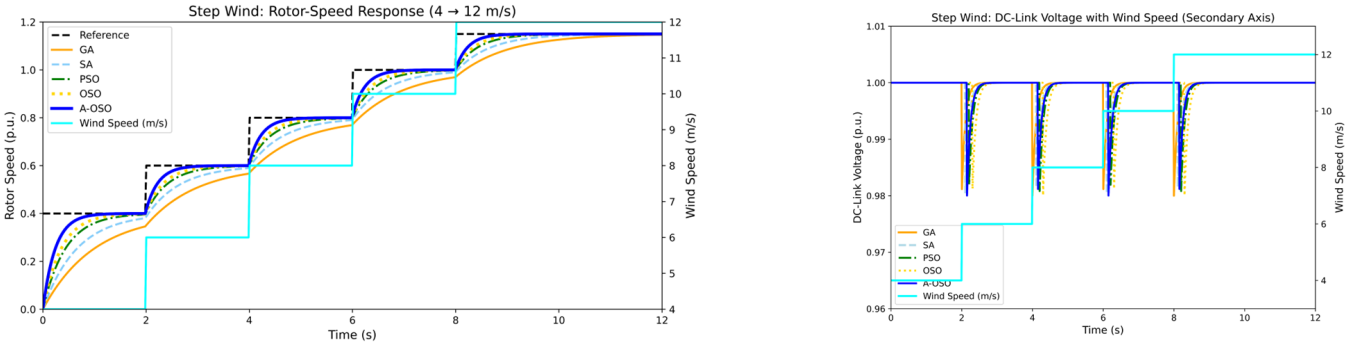
Overview and Baselines

The authors evaluated the proposed A-OSO against GA, SA, PSO, and non-adaptive OSO in both simulation and HIL. The study assessed the power quality via current THD at the PCC (windowed FFT) and power factor. Efficiency and losses used P_{Loss}, (converter conduction/switching plus machine copper losses) and net efficiency η. Fault resilience was measured by $LVRT_{SCORE}$ peak currents/voltages, and post-sag recovery time. For statistics, each scenario was repeated $n = 10$ with varied seeds; the study reports the mean $\pm$ standard deviation and test significance with paired comparisons at $\alpha = 0.05$. Across all scenarios, A-OSO achieved the best overall trade-off, as shown in Table 1.

Table 1. Key performance comparison of A-OSO vs. baseline optimisers across all scenarios.

Methods	Efficiency (%)	THD (%)	LVRT Recovery (ms)	Iteration/Adaptation Round
A-OSO	97.1 +/− 0.2	2.4 +/− 0.1	145 +/− 12	65 +/− 6
OSO	95.5 +/− 0.3	2.9 +/− 0.1	170 +/− 15	85 +/− 7
PSO	94.8 +/− 0.3	3.1 +/− 0.1	180 +/− 18	90 +/− 9
SA	93.2 +/− 0.4	3.8 +/− 0.2	220 +/− 20	110 +/− 10
GA	92.5 +/− 0.5	4.5 +/− 0.3	300 +/− 28	120 +/− 11

Figure 3a shows that an A-OSO delivers the fastest, cleanest tracking under 4 → 6 → 8 → 10 → 12 m/s steps, short rise/settling, and <3% overshoot, while OSO/PSO lag slightly and GA/SA show longer settling and larger peaks (notably at 6 → 10 m/s). The DI quickly shifts to exploitation after each peak, tightening the response envelope and minimising inter-step drift. Figure 3b shows that all controllers hold ~1.0 p.u., but A-OSO exhibits the smallest ripple and the fastest recovery (≲150 ms) after each wind step. OSO/PSO exhibit longer tails, while SA/GA have deeper dips and slower returns. This tighter DC-link regulation reduces GSC stress and supports superior power-quality KPIs.

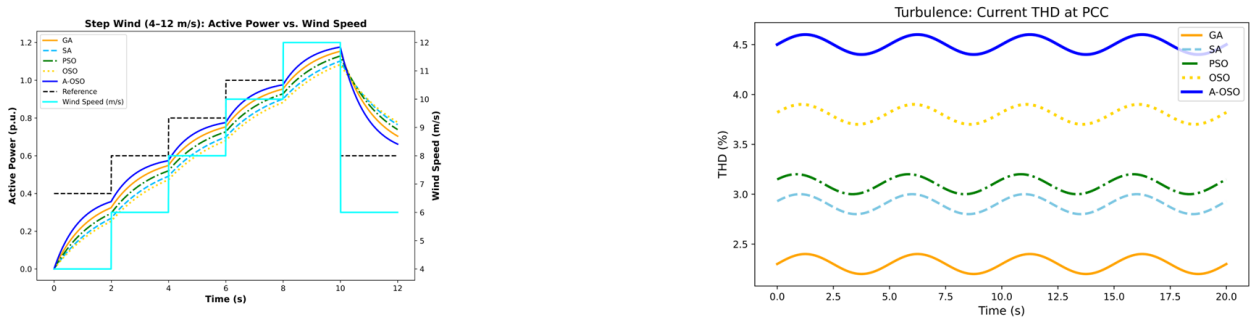


(**a**) (**b**)

Figure 3. (**a**) Step wind: rotor-speed response vs. time. (**b**) Step wind: DC link-voltage response vs. time.

Figure 4a evaluates active-power tracking under step wind speed variations (4–12 m/s). Performance is quantified using 10–90% rise time and 2% settling time; the AOSO-tuned PI achieves the shortest settling times and the lowest steady-state error without overshoot. The smoother transitions result from enforced current and torque-rate constraints that prioritise stable recovery and reduce transient current stress. Figure 4b shows that the AOSO-tuned PI consistently achieves the lowest THD under turbulent conditions, whereas SA and GA exhibit higher distortion levels. The reduction is due to improved converter

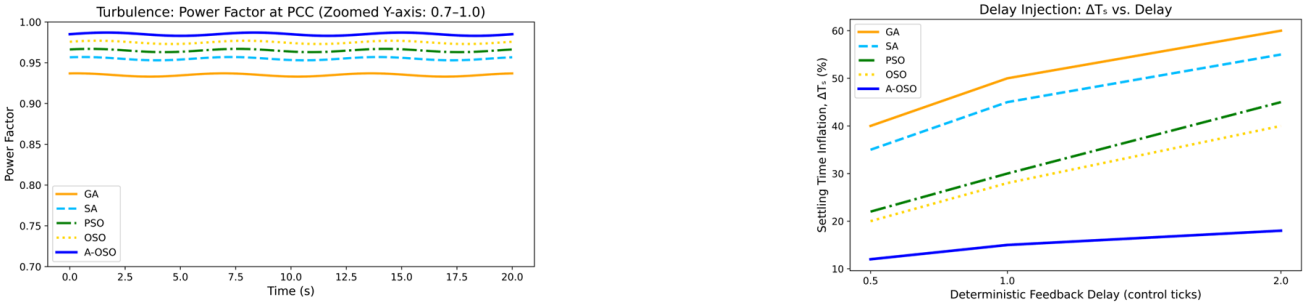
current regulation and the damping of oscillatory responses. Mean and maximum THD values confirm the superior power-quality performance of the proposed method.



(**a**) (**b**)

Figure 4. (**a**) Active power response comparison among the controllers. (**b**) Turbulence: current THD vs. time.

The controller regulates the power factor by controlling the q-axis current and adjusting reactive power at the PCC. As shown in Figure 5a, the AOSO-tuned PI maintains the highest and most stable PF over the 20 s interval, indicating more effective reactive-power compensation than SA, GA, PSO, and OSO. Figure 5b further demonstrates that deterministic feedback delays of 0.5–2 control ticks increase settling time for all methods; however, A-OSO exhibits the lowest sensitivity (+12/+15/+18%) compared with OSO, PSO, SA, and GA. This robustness arises from the DI-triggered transition to exploitation following transient peaks, which damps delay-induced ringing and prevents loop re-excitation.



(**a**) (**b**)

Figure 5. (**a**) Turbulence: Power factor at PCC vs. time. (**b**) Delay injection (ΔTs vs. deterministic feedback delay).

5. Comparative Performance and Discussion

The comparative results summarise performance and computational cost across all methods. Figure 6a presents a normalised radar chart combining efficiency, THD, settling time T_s, and LVRT recovery, where larger areas indicate better overall performance. The proposed A-OSO encloses the largest and most balanced polygon, achieving simultaneous improvements in efficiency, power quality, transient response, and fault recovery, while OSO and PSO show moderate contraction (mainly in THD and LVRT), and SA/GA degrade markedly in T_s and LVRT.

Figure 6b further shows that A-OSO requires the least computational effort, averaging 65 iterations per round, compared with 85–120 for the benchmarks, resulting in a 24–46% reduction in evaluations. Across key performance indicators, A-OSO consistently outperforms all methods, achieving 97.1% efficiency, 2.4% THD, and LVRT recovery of approximately 145 ms. These gains stem from DI-triggered adaptive exploration, which

allocates computation during disturbances and contracts the search under steady conditions. Step-wind and turbulence tests confirm tightened transients, sustained PF above 0.97, and low THD, while HIL results closely match simulations, validating real-time feasibility. Remaining limitations include average-value modelling, heuristic DI formulation, and evaluation on a single DFIG rating, which motivate future work on higher-fidelity models and broader validation.



(**a**) (b)

Figure 6. (**a**) The radar chart groups KPIs, efficiency, THD, settling time, and LVRT recovery. (**b**) Comparative performance metrics.

6. Conclusions and Future Work

The authors propose an A-OSO framework for the online PI tuning of DFIG RSC/GSC loops. Novelties: (i) A disturbance-aware exploration–exploitation balance via an online DI; (ii) a multi-objective cost that jointly targets dynamics, efficiency, THD, and explicit LVRT compliance; and (iii) HIL real-time validation. Across steps, turbulence, LVRT, and cyber impairments, an A-OSO achieves the best overall KPIs ($\eta \approx 97.1\%$, THD $\approx 2.4\%$, LVRT ≈ 145 ms) with the lowest average computational complexity among metaheuristics, making it practical for embedded, grid-code-oriented deployment. Future work: Objectives include thermal/lifetime stress and Pareto tracking; learned DI features/thresholds; event-triggered budgeting with certified WCET; full-switching models and longer field datasets; extensions to PMSG/PV/STATCOM and non-PI (e.g., MPC); and integrated anomaly detection with graceful degradation for stronger cyber-resilience.

Author Contributions: Conceptualisation, R.K.B. and A.K.S.; methodology, R.K.B.; software, R.K.B.; validation, A.K.S.; data curation, R.K.B.; writing—original draft preparation, R.K.B.; writing—review and editing, R.K.B.; supervision, A.K.S.; project administration, A.K.S.; funding acquisition, A.K.S. All authors have read and agreed to the published version of the manuscript.

Funding: This research received no external funding.

Institutional Review Board Statement: Not applicable.

Informed Consent Statement: Not applicable.

Data Availability Statement: Data is embedded in the article.

Conflicts of Interest: The authors declare no conflicts of interest.

References

1. Benbouhenni, H.; Yessef, M.; Bizon, N.; Kadi, S.; Bossoufi, B.; Alhejji, A. Hardware-in-the-loop simulation to validate the fractional-order neuro-fuzzy power control of variable-speed dual-rotor wind turbine systems. *Energy Rep.* **2024**, *11*, 4904–4923. [CrossRef]
2. Biyazne, L.W.; Tuka, M.B.; Abebe, Y.M.; Wellhöfer, A. Enhancing MPPT performance of a grid-connected Doubly-Fed induction generator-based wind power plant using hybrid ANFIS-PI control strategy. *Sci. Rep.* **2026**, *16*, 5732. [CrossRef] [PubMed]

3. Behara, R.K.; Saha, A.K. Analysis of Wind Characteristics for Grid-Tied Wind Turbine Generator Using Incremental Generative Adversarial Network Model. *IEEE Access* **2024**, *12*, 38315–38334. [CrossRef]
4. Hosseini, E.; Al-Ghaili, A.M.; Kadir, D.H.; Gunasekaran, S.S.; Ahmed, A.N.; Jamil, N.; Deveci, M.; Razali, R.A. Meta-heuristics and deep learning for energy applications: Review and open research challenges (2018–2023). *Energy Strateg. Rev.* **2024**, *53*, 101409. [CrossRef]
5. Hadj Slama, A.; Saidi, L.; Saidi, M.; Benbouzid, M. Metaheuristic Optimization of Hybrid Renewable Energy Systems Under Asymmetric Cost-Reliability Objectives: NSGA-II and MOPSO Approaches. *Symmetry* **2025**, *17*, 1412. [CrossRef]
6. Behara, R.K.; Saha, A.K. Artificial intelligence techniques framework in the design and optimisation phase of the doubly fed induction generator's power electronic converters: A review of current status and future trends. *Renew. Sustain. Energy Rev.* **2025**, *215*, 115573. [CrossRef]
7. Nasim, F.; Khatoon, S.; Ibraheem; Urooj, S.; Shahid, M.; Ali, A.; Nasser, N. Hybrid ANFIS-PI-Based Optimization for Improved Power Conversion in DFIG Wind Turbine. *Sustainability* **2025**, *17*, 2454. [CrossRef]
8. Xu, J.; Feng, P.; Gong, J.; Li, S.; Jiang, G.; Yang, H. Low-Voltage Ride-Through Strategy to Doubly-Fed Induction Generator with Passive Sliding Mode Control to the Rotor-Side Converter. *Energies* **2024**, *17*, 4439. [CrossRef]
9. Preus, R.; Reilly, J.; Johnson, J.; Baring-gould, I.; Coddington, M.; Preus, R.; Reilly, J.; Johnson, J.; Baring-gould, I.; Coddington, M. *Distributed Wind Considerations from the IEEE 1547-2018 Revision Distributed Wind Considerations From the IEEE 1547-2018 Revision*; IEEE: New York, NY, USA, 2021.
10. Sai, B.S.V.; Chatterjee, D.; Mekhilef, S.; Wahyudie, A. An SSM-PSO Based MPPT Scheme for Wind Driven DFIG System. *IEEE Access* **2022**, *10*, 78306–78319. [CrossRef]
11. Mahvash, H.; Taher, S.A.; Guerrero, J.M. Modified backstepping control for cyber security enhancement of a wind farm based DFIG against false data injection, hijack and denial of service cyber attacks. *Electr. Power Syst. Res.* **2024**, *231*, 110357. [CrossRef]
12. Jain, M.; Maurya, S.; Rani, A.; Singh, V. Owl search algorithm: A novel nature-inspired heuristic paradigm for global optimization. *J. Intell. Fuzzy Syst.* **2018**, *34*, 1573–1582. [CrossRef]
13. Ilchi Ghazaan, M.; Salmani Oshnari, A.; Salmani Oshnari, A. A novel adaptive optimization scheme for advancing metaheuristics and global optimization. *Swarm Evol. Comput.* **2024**, *91*, 101779. [CrossRef]
14. Xiang, X.; Diao, R.; Bernadin, S.; Foo, S.Y.; Sun, F.; Ogundana, A.S. An Intelligent Parameter Identification Method of DFIG Systems Using Hybrid Particle Swarm Optimization and Reinforcement Learning. *IEEE Access* **2024**, *12*, 44080–44090. [CrossRef]
15. Abood, S.; Annamalai, A.; Khalid, I.; Chouikha, M.; Al-Zuhairi, H.A. AI-Based Hybrid Control for Optimizing Doubly-Fed Induction Generators in Wind Turbines. *Int. J. Intell. Eng. Syst.* **2025**, *18*, 439–459. [CrossRef]
16. Elnaghi, B.E.; Abelwhab, M.N.; Abdel-Kader, F.E.S.A.; Ismaiel, A.M.; Mohammed, R.H.; Dessouki, M.E. Experimental Validation of Second-Order Adaptive Fuzzy Logic Controller for Grid-Connected DFIG Wind Power Plant. *IEEE Access* **2023**, *11*, 135255–135271. [CrossRef]
17. Lazo, Y.; Crawford, B.; Cisternas-Caneo, F.; Barrera-Garcia, J.; Soto, R.; Giachetti, G. Evolution and Trends of the Exploration–Exploitation Balance in Bio-Inspired Optimization Algorithms: A Bibliometric Analysis of Metaheuristics. *Biomimetics* **2025**, *10*, 517. [CrossRef] [PubMed]

Disclaimer/Publisher's Note: The statements, opinions and data contained in all publications are solely those of the individual author(s) and contributor(s) and not of MDPI and/or the editor(s). MDPI and/or the editor(s) disclaim responsibility for any injury to people or property resulting from any ideas, methods, instructions or products referred to in the content.